International Journal of Energy Research

INTERNATIONAL JOURNAL OF ENERGY RESEARCH
Int. J. Energy Res. 2015; **39**:2053–2061
Published online 23 October 2015 in Wiley Online Library (wileyonlinelibrary.com). DOI: 10.1002/er.3441

Energy storage in symmetric and asymmetric supercapacitors based in carbon cloth/polyaniline–carbon black nanocomposites

Marcela A. Bavio[1,2,*,†], Gerardo G. Acosta[1,2] and Teresita Kessler[1]

[1]Facultad de Ingeniería, INTELYMEC-CIFICEN, UNCPBA. Av. del Valle 5737, Olavarría, Buenos Aires, Argentina
[2]CONICET, Av. Rivadavia 1917, Ciudad Autónoma de Buenos Aires C1033AAJ, Argentina

SUMMARY

In this work, the construction of electrochemical capacitors using polyaniline–carbon black nanocomposites as electrode material is described. Symmetric and asymmetric cells were assembled. The active material was supported on carbon cloth acting as current collector as well. The electrolyte was H_2SO_4 0.5 M, and the selected potential range was 1 V. The electrochemical behavior of the arrayed supercapacitors was studied by cyclic voltammetry and galvanostatic charge/discharge runs. At a constant current density of 0.3 A/g, a specific capacitance value of 1039 F/g was obtained for a symmetric assembly using both electrodes prepared with polyaniline and carbon black nanocomposites. When the set is asymmetric, being the positive electrode made of polyaniline and carbon black nanocomposites, the specific capacitance value is 1534 F/g. For the latter array, the specific power and energy density values are 300 W/kg and 426 Wh/kg at 0.3 A/g, and 13 700 W/kg and 28 Wh/kg at 13.7 A/g. These results suggest a good capacity of fast energy transfer. Moreover, this asymmetric supercapacitor demonstrated a high stability over 1000 cycles being the loss of only 5%.

KEY WORDS

supercapacitors; symmetric and asymmetric cell assemblies; nanocomposites; energy storage

Correspondence

*Marcela A. Bavio, Facultad de Ingeniería, INTELYMEC-CIFICEN, UNCPBA, Av. del Valle 5737, Olavarría, Buenos Aires, Argentina.
†E-mail: mbavio@fio.unicen.edu.ar

Received 8 May 2015; Revised 15 September 2015; Accepted 18 September 2015

1. INTRODUCTION

The industrial and technological development requires a great amount of available energy. Nowadays, the mean energy source depends on non-renewable reservoirs such as natural gas, coal and oil, whose recollection is turning to be difficult because of their location. Moreover, their use generates contaminants that modify the environment and affect the weather, causing economical complications as well. These are severe reasons that motivate the research of other ways to obtain energy in a more friendly way and less contaminant to the surroundings, such as solar or wind energy. The main disadvantages of these energy systems are related to their relatively high construction and maintenance costs, and the energy storage restriction. Hence, systems allowing energy storage and preservation, like batteries and capacitors cells, sum up to solve the energy problem. In recent years, the supercapacitors (called also electrochemical capacitors or ultracapacitors) have emerged as an alternative or an adjunct to conventional capacitors and batteries [1–3].

The main advantages of supercapacitors are longer life than rechargeable batteries, excellent cyclability, high efficiency in charge–discharge cycles, low maintenance costs, ability to provide energy very quickly and to operate in extreme temperatures and the use of less toxic components compared with other energy storage devices [4]. In supercapacitors, it is important to consider not only the amount of electricity that they are capable to store but also their maximum power that is usually higher than conventional batteries and conventional dielectric capacitors [5].

Many different materials are employed as electrodes in supercapacitors. They can be classified into three types: carbonaceous materials (carbon nanotubes (CNT), activated carbon, carbon black (CB) and graphene), transition metal oxides (single or mixed Ru, Ni, Mn and Co oxides) and conductive polymers (polyaniline (PANI), polythiophene and polypyrrole) [6–10]. From our previous studies, it was established that nanocomposites made of pure PANI or PANI with the addition of CB have good capacitance, power and energy values, reporting specific capacitance values of

1486 F/g and 1744 F/g for PANI nanostructures and PANI–CNT nanocomposites, respectively [11,12]. Other researchers have informed similar specific capacitance values for different PANI nanostructures varying the method of synthesis, particle size, porosity and experimental conditions. Specific capacitances ranging 200–2300 F/g were calculated for PANI nanostructures [13–16], and varying between 200 and 600 F/g when employing PANI–CNT nanocomposites [12,14,15]. Moreover, higher specific capacitance values were informed for PANI electrodeposited on carbon based materials such as carbon fiber cloth (1026.8 F/g), vertically aligned CNT (1030 F/g) and porous carbon bars (1600 F/g) [17–19].

Most recently, exciting progress has been made in exploring hybrid nanostructured materials that combine advantages of both electrical double-layer capacitors and pseudocapacitors to improve energy density values while maintaining their high power capability. In order to reach high power and high energy density values simultaneously, novel support structures have been developed for high mass loading of active materials and effective utilization of their electrochemical properties. But the composites of pseudocapacitive and carbonaceous materials are promising electrode materials for ECs because of their good electrical conductivity, low cost and high mass density [2,20].

Nowadays markets offer various types of supercapacitors, mainly in symmetric arrangement using carbonaceous materials as electrodes. However, asymmetric supercapacitors are being also developed, using other nanostructured materials. Asymmetric supercapacitors were prepared with mesoporous carbon/PANI and mesoporous carbon nanocomposites as positive and negative electrodes, respectively, reaching 87.4 F/g in 1 M H_2SO_4 [21]. Furthermore, symmetrical supercapacitors were arranged using porous Ni and NiO, and asymmetric assemblies using activated carbon as the negative electrode and porous Ni or NiO as the positive electrode, obtaining capacitance values of 20 and 40 F/g, respectively, both explored in basic electrolyte [22].

Another type of device is the so-called flexible super capacitor. An example of this arrangement was constructed using CB/graphene films as electrodes and membranes of polyvinyl alcohol/H_2SO_4 [6]. A different configuration was presented arranging a flexible stainless steel mesh with commercial ink as electrodes attaining specific capacitance values of 107.8 F/g [23]. A free-standing flexible supercapacitor was fabricated by sandwiching a polyvinyl alcohol hydrogel polymer electrolyte between two layers of the as-prepared ternary nanocomposite electrodes. This achieved a specific capacitance of 123.8 F/g at 1 A/g [24].

In this work symmetric and asymmetric supercapacitors are assembled using PANI and PANI–CB nanocomposites as electrode material and a carbon cloth acting as support and current collector as well. Their performances were studied by electrochemical techniques, in sulfuric acid.

2. EXPERIMENTAL

2.1. Electrode materials

PANI nanostructures and PANI and CB nanocomposites (PANI–CB) were used to make the negative and/or positive electrodes of the cell.

The PANI nanostructures were chemically synthesized from a dispersion prepared with 0.045 g of aniline, 0.30 mL of 0.25 M HCl and 0.005 g of sodium dodecyl sulfate (SDS) in 18 mL of distilled water under constant magnetic stirring at room temperature (25 °C) for 20 min. Then, 2 mL of 0.24 M ammonium persulfate (APS) was added to the initial mixture. The resulting dispersion was stirred violently for half a minute. The polymerization process was carried out for 24 h at 25 °C without agitation. The obtained precipitate was filtered and washed until the filtrate solution became colorless. Finally, the residue was dried for 24 h at 60 °C. PANI–CB nanocomposites were synthetized applying the same procedure with the addition of 0.1 mg/mL of either functionalized CB (CBf) or non-functionalized CB (CBnf) to the initial aqueous dispersion. CB used was Vulcan XC-72R.

The applied pre-treatment consisted in adding CB particles to 2.2 M nitric acid at room temperature. After stirring the preparation with an ultrasonic bath, it was kept at room temperature for 20 h, then filtered and washed to achieve neutral pH in the filtrate solution. Finally, the residue consisting in CBf particles was dried at 37 °C for 2 h.

PANI nanostructures and PANI–CB nanocomposites were properly characterized by transmission electron microscopy (TEM), scanning electron microscopy (SEM), Fourier transform infrared spectroscopy (FTIR), ultraviolet visible spectroscopy (UV–Vis) and X-ray diffraction [11].

2.2. Preparation of the electrodes

The electrode assembly is shown in Figure 1.a. Carbon cloth (plain Excel®) was used as support and current collector, with a geometric area of 1.5 cm^2. The synthetized materials were deposited on one side of the film from their dispersion in isopropyl alcohol and distilled water. Afterwards, they were dried at room temperature. Successive depositions were performed until the total material load was 1.5 mg/cm^2. Then, a 5% Nafion solution was added, and again, the electrode was dried at room temperature for 30 min. The back side of the carbon cloth was sealed with a Teflon® fabric adhesive.

The electrodes with CB nanoparticles were prepared similarly, using the same load of total, namely 1.5 mg/cm^2.

2.3. Assembly of cells

The electrochemical runs were performed in a two electrodes vial of 20 ml (Figure 1.b), with H_2SO_4 0.5 M as electrolyte. Various cell configurations with different electrodes as anodes and cathodes were tested, giving rise to symmetrical or asymmetrical arrangements, as shown in Table I. The electrode separator was filter paper which

Int. J. Energy Res. 2015; **39**:2053–2061 © 2015 John Wiley & Sons, Ltd.
DOI: 10.1002/er

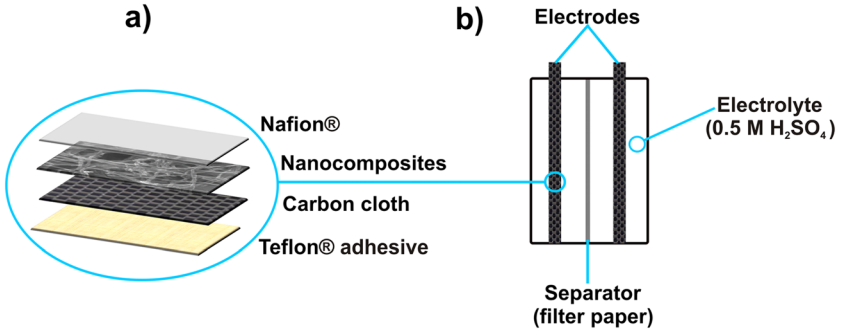

Figure 1. Electrodes and cell design.

Table I. Different cell configurations for symmetric and asymmetric supercapacitors.

Nomenclature	Anode	Cathode
S1	CC–PANI	CC–PANI
S2	CC–PANI–CBs	CC–PANI–CBs
S3	CC–PANI–CBf	CC–PANI–CBf
A1	CC–PANI	CC–CB
A2	CC–PANI–CBs	CC–CB
A3	CC–PANI–CBf	CC–CB

was soaked in the electrolyte for 30 min before use. The cell was purged bubbling N_2 for 10 min and then, sealed before starting the electrochemical measurements.

2.4. Evaluation of supercapacitors

Cyclic voltammetry and galvanostatic measurements were applied to evaluate the performance of the supercapacitors. Runs were carried out in the potential range of 0.0 to 1.0 V. I/V profiles were recorded varying the sweep rate from 10 to 100 mV/s. The charge/discharge experiences were made at different current density values, between 0.3 and 13.7 A/g. All the experiments were performed using a potentiostat/galvanostat EG & G PAR Model 362, coupled to a Nicolet oscilloscope with an acquiring data switch connected to a PC.

From the galvanostatic measurements, parameters such as the specific capacitance of the material (Cm), the specific energy (Es), the specific power (Ps) and the coulombic efficiency (η) were calculated, applying by the following equations, 1 to 4, respectively:

$$C_m = 2\frac{C}{m} = 2\frac{I\ \Delta t_d}{\Delta V\ m} \quad (1)$$

$$E_s = \frac{I\ \Delta V\ \Delta t_d}{m} \quad (2)$$

$$P_s = \frac{I\ \Delta V}{m} \quad (3)$$

$$\eta = \frac{\Delta t_d}{\Delta t_c} \cdot 100\% \quad (4)$$

where C is the experimental capacitance value, I is the charge/discharge current, Δt_d is the download established time, ΔV is the potential range, m is the mass of a composite employed as electrode and Δt_c is the charging time [6,22,25].

3. RESULTS AND DISCUSSION

3.1. Nanostructures of PANI and PANI–CB

Figure 2 shows SEM and TEM micrographs of different PANI and PANI–CB nanostructures. PANI nanotubes of ca. 15-μm length and an outer diameter of 95 nm (Figure 2a) are obtained when synthetizing aniline solution without additions.

The addition of CBf particles promotes the development of nanostructures with different shapes such as nanobelts and nanotubes (Figure 2b). PANI–CBf nanobelts have a thickness of ca. 100 nm, a width of 2 μm and a length of 12–15 μm. PANI–CBf nanotubes have a mean outside diameter of ca. 95 nm and a length of 15 μm. On the other hand, when adding CBnf particles, the development of various nanostructures is evident: nanotubes (diameter: 95 nm, length: 5–8 microns), nanoparticles (diameter: 85–90 nm) nanobelts (length: 10–12 microns, width: 1 micron and thickness: 100 nm) and nanosheets (length: 0.5 microns, width: 0.3 microns and thickness: 95–100 nm) (Figure 2c).

The FTIR (Figure 2 d) results show several bands that appear in all the PANI nanostructures spectra [11,26,27]. The position of the common bands and the corresponding assignment are stated as follows: 1142 cm^{-1} (assigned as —N=quinoid=N—), 1305 cm^{-1} (CN stretching with aromatic conjugation), 1498 and 1585 cm^{-1} (C=C stretching in benzoides and quinoid rings respectively), and 2847 and 2916 cm^{-1} (CH stretching of —CH_3 and —CH_2—, respectively, which shows the presence of SDS in the synthesized products).

In the nanostructure spectra, a distinguishable band is present at 1042 cm^{-1}; it is attributed to the substitution of S=O groups in the 1,2,4-aromatic rings, indicating a doped PANI structure as a result of using APS during the synthesis. These results agree with the EDS results, where the presence of S was determined. Another band located at 3250 cm^{-1} is assigned to NH stretching associated to different intra- and inter-molecular hydrogen

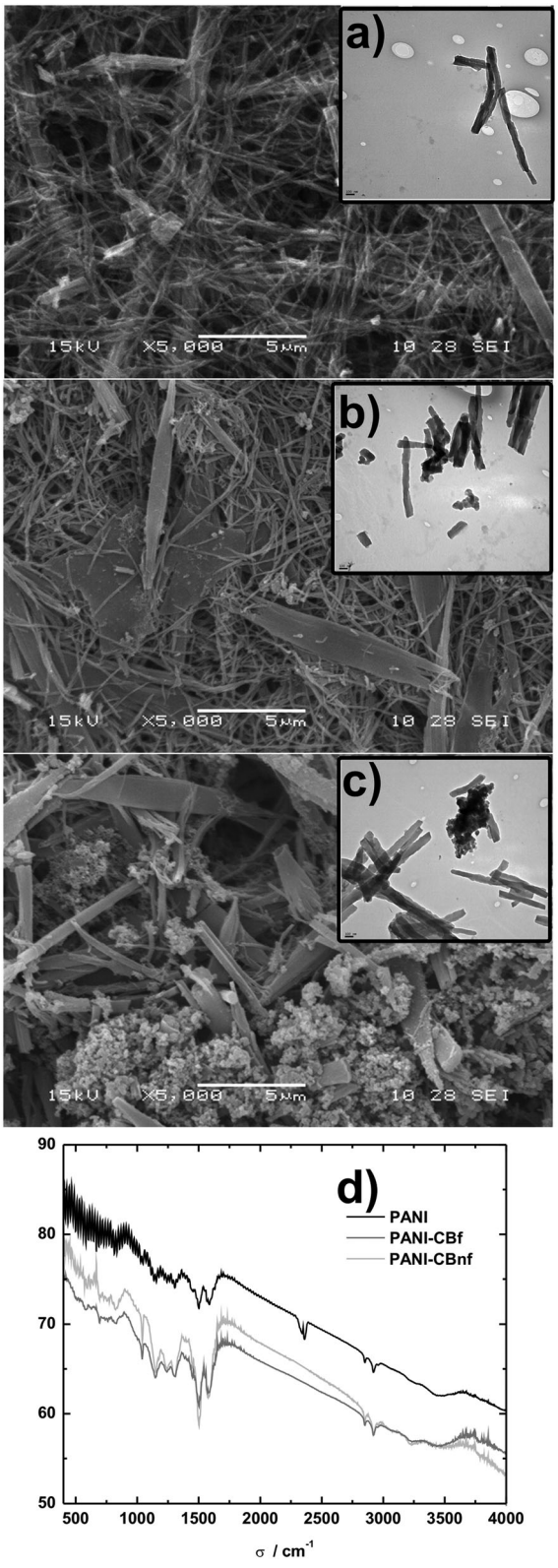

Figure 2. SEM and TEM (inset) images of a) PANI, b) PANI–CBf and c) PANI–CBnf nanostructures. d) FTIR spectra.

bonds in secondary amines. In the presence of a sulfonate group, a hydrogen bond such as the NH—O type can be proposed. These results are consistent with those found in the analysis by UV–Vis spectroscopy, confirming the presence of groups that tend to form hydrogen bonds.

Furthermore, other bands must be indicated as contributions to the final formation of the nanostructures, including the ones located at 825 cm^{-1} (CH deformation out of plane in benzoides rings), at 692 cm^{-1} (CC out of plane deformation of rings monosubstituted aromatic), at 1242 cm^{-1} (CN stretching of secondary aromatic amines) and at 1446 cm^{-1} (presence of branched structures such as phenazine) [11,28,29].

3.2. Cyclic voltammetry

The voltammograms, at different scan rates, corresponding to the symmetric and asymmetric arrangement of the developed electrodes are shown in Figure 3 (a,b,c) and Figure 3 (d,e,f), respectively. It is to point out their almost capacitive behavior as the voltammograms in their anodic and cathodic runs are not completely symmetric and rectangular shaped as the purely capacitive behavior would denote. This fact may be attributed to a pseudocapacitive contribution corresponding to the conductive polymer incorporated as electrode material.

All voltammograms presented high current density and no evident current peaks, indicating good electrochemical activity and high power density.

The specific capacitance values were calculated from the voltammograms using the following equation:

$$Cs = \frac{\int_{V_1}^{V_2} I(V)dV}{(V_2 - V_1)\,v \cdot m} \tag{5}$$

where I is the current in the I/V profiles, $\int_{V_1}^{V_2} I(V)dV$ is the area under the curve I/V, v is the scanning rate, $(V_2 - V_1)$ is the potential window and m is the mass of the electroactive material [30].

The calculated capacitance values are presented in Table II for the asymmetric and symmetric assemblies with the electrode materials listed in Table I. Comparing the capacitance values for the various asymmetric arrangements, the best results are obtained with electrodes prepared from PANI–CBf nanocomposites at any scan rate. For the symmetric supercapacitors, this trend is not so notable. According to these results it can be established that the asymmetric conformation provides higher capacitance values compared to the symmetric assembly when the electrodes have CB or CBf. In the case of electrodes containing PANI nanostructures, the symmetric configuration provided the higher capacitance values.

Int. J. Energy Res. 2015; **39**:2053–2061 © 2015 John Wiley & Sons, Ltd.
DOI: 10.1002/er

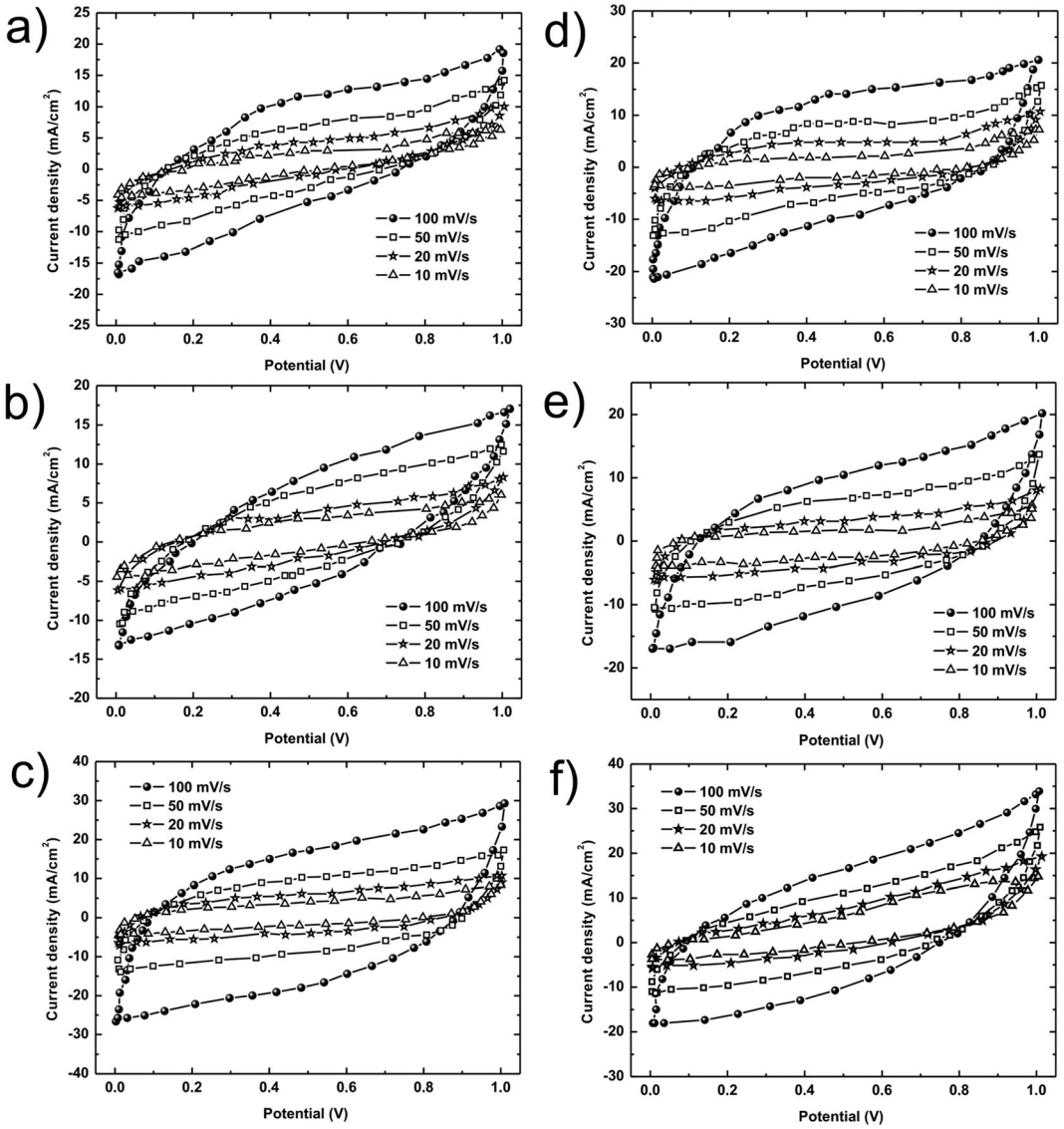

Figure 3. Cyclic voltammograms obtained at different scan rates for symmetric S1 a), S2 b) and S3 c) and asymmetric A1 d), A2 e) and A3 f) supercapacitors.

Table II. Specific capacitances for the symmetric and asymmetric supercapacitors calculated from the cyclic voltammetry at different scan rates.

Scan rate mV/s	Specific capacitance F/g					
	A1	A2	A3	S1	S2	S3
10	429	517	901	477	485	1013
20	365	384	495	436	352	320
50	260	237	360	292	224	379
100	211	182	330	234	162	283

The specific capacitance values increase as scan rate decreases. The maximum specific capacitances at low scan rate were obtained with S3 and A3 assemblies, namely 1013 and 901 F/g respectively.

3.3. Galvanostatic measurements

Galvanostatic charge/discharge measurements were carried out at different current densities between 0.3 and 13.7 A/g, in the voltage range from 0.0 to 1.0 V in order to evaluate the charge storage capacity, cycling life, efficiency and other electrical parameters such as the specific power (Ps) and specific energy (Es).

Figure 4 shows the galvanostatic profiles of some asymmetric (Figure 4.a) and symmetric (Figure 4.b) supercapacitor assemblies at 0.3 A/g.

A non-linear discharge curve was revealed for most of the prepared supercapacitors. In the symmetric supercapacitors this effect is more pronounced. It can be explained taking into account the existence of a redox reaction in the same voltage range [31].

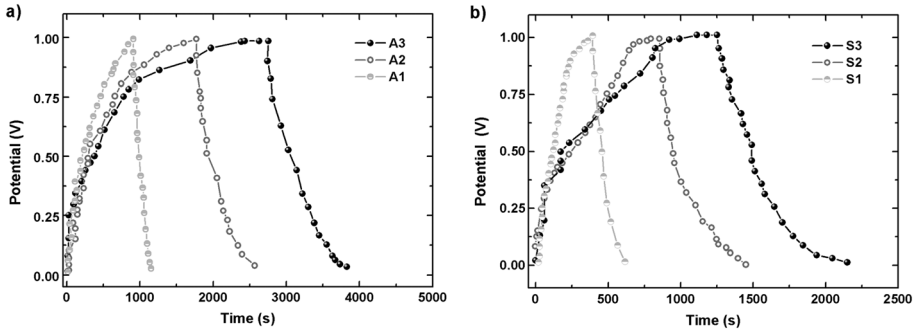

Figure 4. Representative galvanostatic charge–discharge curves for the asymmetric (a) and symmetric (b) supercapacitors at 0.3 A/g.

When the responses of the asymmetric supercapacitors are evaluated, there is no significant voltage drop (*IR drop*) during the initial stage of the download process. They present a more linear profile in comparison to symmetric supercapacitors. This fact indicates that the internal resistance of the asymmetric supercapacitors is less than the symmetrical supercapacitor resistance. Thus, electrochemical parameters of the asymmetric supercapacitors are greater than the symmetrical. The equivalent series resistance includes ohmic resistance of the electrolytes, resistances from the cell design, for example, components and contact resistance between current collectors and electrodes. Internal resistance may be decreased because of the use of less resistive materials as black carbon electrodes and to the formation of an electrode/electrolyte interface with good conductivity [3,22]. The advantage of this design of supercapacitors is then the reduction of internal resistance, because the current collectors are involved directly in the electrode, allowing reducing the contact resistance between the current collector and the electrode.

The specific capacitances of the supercapacitors in relation to the applied charge/discharge current were calculated and presented in Table III. It was observed that the capacitance values, calculated either for the symmetric or asymmetric configuration, showed the greatest values when the nanocomposites used as electrode material contained CBf nanoparticles. In all the cases, an increase in the specific capacitance is noted as the charge/discharge current diminished. A significant decrease from 1534 F/g to 100 F/g can be observed when the current increases 0.3 A/g to 13.7 A/g for the A3 supercapacitor and decreased 1039 F/g to 77 F/g for the S3 supercapacitor in the same current density range.

Table III. Specific capacitances for the symmetric and asymmetric supercapacitors calculated from galvanostatic charge/discharge curves at different current density values.

Current density (A/g)	Specific capacitance (F/g)					
	A1	A2	A3	S1	S2	S3
0.3	628	1290	1534	497	846	1039
0.7	546	569	788	354	517	600
1.3	394	425	466	260	306	403
3.3	236	260	363	200	180	280
6.7	110	236	251	76	149	170
13.7	29	56	100	68	69	77

The specific capacitance values obtained from the galvanostatic runs were slightly higher, compared with those obtained from the cyclic voltamperometry experiment for the asymmetric supercapacitor. For the symmetric cells there is a good correlation between CV and galvanostatic measurements. However, comparing to the values previously reported, the actual results are lower. This may be because of the use of different current collectors and the geometrical factors of the electrochemical cell that in the present case provokes a high ionic resistance within the pores of the carbon cloth which leads to a decrease in the capacitance values [11].

It was also probed that the asymmetric supercapacitors offer higher capacitance values than its symmetrical configuration. In both arrangements, the inclusion of CBf improves the specific capacitance from 629 F/g to 1534 F/g when comparing A1 and A3 asymmetric assemblies, and from 497 F/g to 1039 F/g for S1 and S3 symmetric configuration. CB particle aggregate to the electrode material also improves specific capacitance values compared to those systems not containing CB, being the effect less pronounced.

Another important parameter to analyze is their efficiency in relation to the applied current density. Thus, at high current density values (13.7 A/g), all the prepared supercapacitors have a charge/discharge efficiency of ca. 85%. On the other hand, at low current densities (0.3 A/g) the symmetric devices maintain a high efficiency, ca. 80%, while for the asymmetric configurations this value falls to ca. 55%.

Int. J. Energy Res. 2015; **39**:2053–2061 © 2015 John Wiley & Sons, Ltd.
DOI: 10.1002/er

The Ragone representation as the relationship between the specific power density and specific energy density is shown for the assembled supercapacitors in Figure 5 [4]. The higher specific energy and power values are obtained for asymmetric supercapacitors (Figure 5.a).When the charge/discharge current density is increased from 0.3 to 13.7 A/g, the energy density decreased from 426.1 to 27.8 Wh/kg in A3, but the power density increased from 300 to 13 700 W/kg. Similar results were obtained for flexible supercapacitors with noncarbonaceous electrode materials [23,32]. The calculated energy density and power density for symmetric supercapacitors are shown in Figure 5.b. Thus, when the power density increased from 300 to 13 700 W/kg, the energy density decreased from 288.6 to 21.4 Wh/kg for the S3 assembly. For all of the prepared supercapacitors, the addition of CB improves the specific capacitance, power density and energy density.

Supercapacitor stability over 1000 charge/discharge cycles was also evaluated. In Figure 6, the specific capacitances of the supercapacitors are presented as a function of the number of cycles, calculated at 0.3 A/g. It was found that the capacitance loss during the charge/discharge process is less than 20% for all the prepared supercapacitors (Figure 6a,b), being the A3 configuration the one with the least loss of capacitance.

These results reveal that the stability of the electrode material can be improved significantly with the addition of CB nanoparticles in the PANI nanostructures.

In summary, the incorporation of CBf in the electrode material improves greatly the performance of all the supercapacitors' assemblies. This effect is enhanced in the asymmetric supercapacitors. In fact the electrochemical parameters for the A3 arrangement are 30% larger than the ones for the S3 assembly. However, all of the constructed devices exhibited a very good stability for 1000 charge/discharge cycles with a retention capacitance of 80–95%, and an efficiency of 80–85% at high current densities. As the major advantages it is to point out that the supercapacitors were manufactured through a simple method; they are robust and can be used in stationary applications.

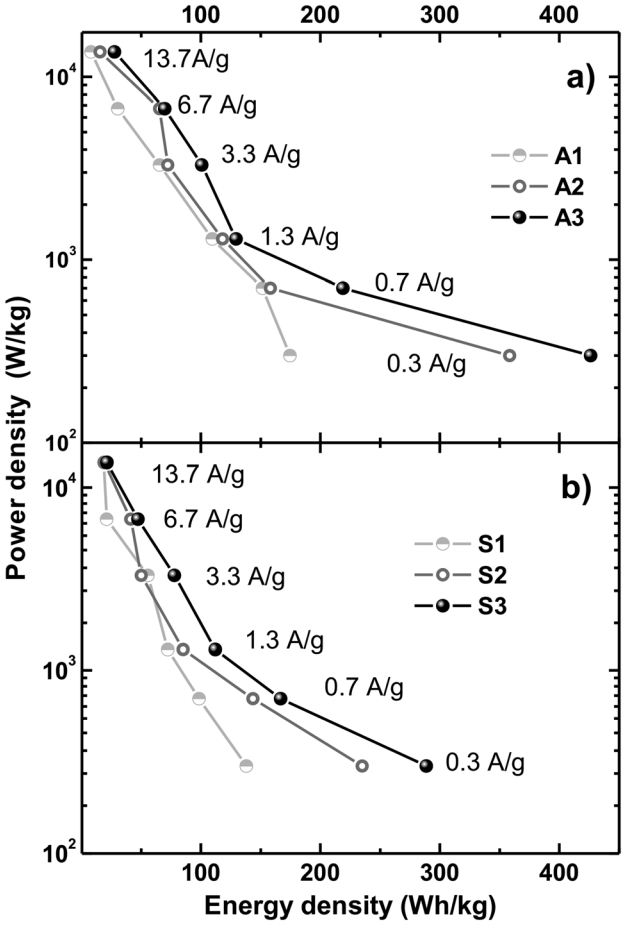

Figure 5. Energy and power densities of the asymmetric (a) and symmetric (b) supercapacitors calculated from the galvanostatic charge/discharge curves at different current densities ranging from 0.3 to 13.7 A/g.

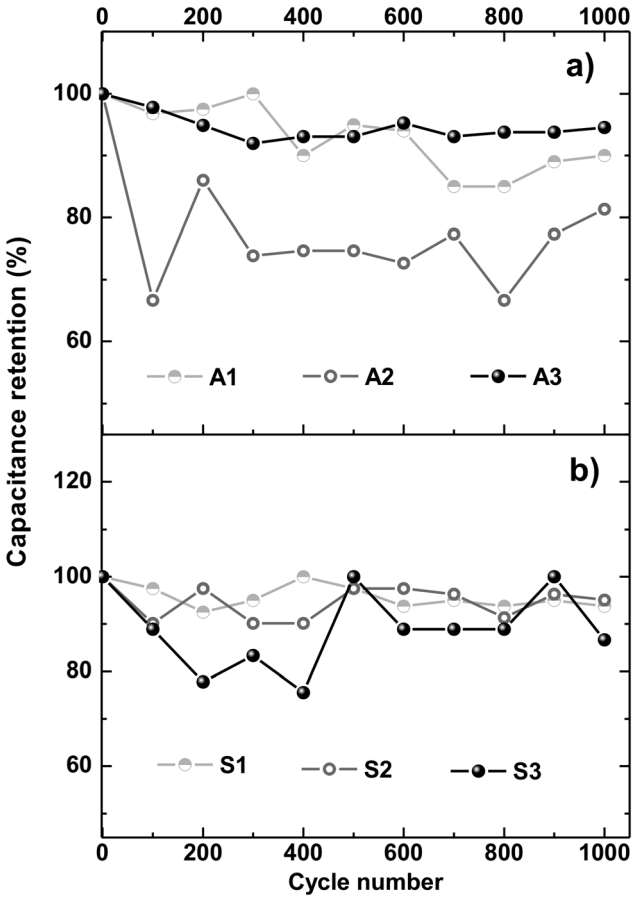

Figure 6. Cycles life test of asymmetric a) and symmetric b) supercapacitors.

4. CONCLUSIONS

Symmetric and asymmetric supercapacitors have been constructed using PANI nanostructures and PANI–CB nanocomposites as electrode materials. Specific capacitance values of the devices were measured using cyclic voltammetry and galvanostatic charge/discharge cycles. The best results were obtained with the asymmetric assembly. The lab scale devices are stable for 1000 charge–discharge cycles, with capacitance retention of 80–95%. The asymmetric supercapacitors prepared incorporating PANI–CBf nanocomposites in the positive electrode and CB nanoparticles in the negative electrode exhibited the best performance in terms of capacitance, energy, power and stability.

REFERENCES

1. Kothari DP, Singal KC, Ranjan R. *Renewable Energy Sources and Emerging Technologies*. PHI Learning Private Limited: India, 2008.
2. Yu G, Xie X, Pan L, Bao Z, Cui Y. Hybrid nanostructured materials for high-performance electrochemical capacitors. *Nano Energy* 2013; **2**:213–234.
3. Kim BK, Sy S, Yu A, Zhang J. Electrochemical supercapacitors for energy storage and conversion. In *Handbook of Clean Energy Systems*. 2015; 1–25.
4. Winter M, Brodd RJ. What are batteries, fuel cells, and supercapacitors. *Chemical Reviews* 2004; **104**: 4245–4269.
5. Burke A. Ultracapacitor technologies and application in hybrid and electric vehicles. *International Journal of Energy Research* 2010; **34**:133–151.
6. Fei H, Yang Ch, Bao H, Wang G. Flexible all-solid-state supercapacitors based on graphene/carbon black nanoparticle film electrodes and cross-linked poly(vinylalcohol)-H_2SO_4 porous gel electrolytes. *Journal of Power Sources* 2014; **266**:488–495.
7. Huang M, Zhang Y, Li F, Zhang L, Wen Z, Liu QJ. Facile synthesis of hierarchical Co_3O_4@MnO_2 core–shell arrays on Ni foam for asymmetric supercapacitors. *Journal of Power Sources* 2014; **252**:98–106.
8. Bian L-J, Luan F, Liu Sh-Sh, Liu X-X. Self-doped polyaniline on functionalized carbon cloth as electroactive materials for supercapacitor. *Electrochimica Acta* 2012; **64**:17–22.

9. Hea X, Gao B, Wang G, Wei J, Zhao Ch. A new nanocomposite: carbon cloth based polyaniline for an electrochemical supercapacitor. *Electrochimica Acta* 2013; **111**:210–215.
10. Mao M, Hu J, Liu H. Graphene-based materials for flexible electrochemical energy storage. *International Journal of Energy Research* 2015; **39**:727–740.
11. Bavio MA, Acosta GG, Kessler T. Polyaniline and polyaniline–carbon black nanostructures as electrochemical capacitor electrode materials. *International Journal of Hydrogen Energy* 2014; **39**:8582–8589.
12. Bavio MA, Acosta GG, Kessler T. Synthesis and characterization of polyaniline and polyaniline–carbon nanotubes nanostructures for electrochemical supercapacitors. *Journal of Power Sources* 2014; **245**:475–481.
13. Mi H, Zhang X, Yang S, Ye X, Luo J. Polyaniline nanofibers as the electrode material for supercapacitors. *Materials Chemistry and Physics* 2008; **112**:127–131.
14. Zhou Y, He B, Zhou W, Huang J, Li X, Wu B, Li H. Electrochemical capacitance of well-coated single-walled carbon nanotube with polyaniline composites. *Electrochimica Acta* 2004; **49**:257–262.
15. Gupta V, Miura N. Influence of the microstructure on the supercapacitive behavior of polyaniline/single-wall carbon nanotube composites. *Journal of Power Sources* 2006; **157**:616–620.
16. Rajendra Prasad K, Munichandraiah N. Fabrication and evaluation of 450 F electrochemical redox supercapacitors using inexpensive and high-performance, polyaniline coated, stainless-steel electrodes. *Journal of Power Sources* 2002; **112**:443–451.
17. Zhang H, Cao G, Wang Z, Yang Y, Shi Z, Gu Z. Tube-covering-tube nanostructured polyaniline/carbon nanotube array composite electrode with high capacitance and superior rate performance as well as good cycling stability. *Electrochemistry Communications* 2008; **10**:1056–1059.
18. Cheng Q, Tang J, Ma J, Zhang H, Shinya N, Qin L. Polyaniline-coated electro-etched carbon fiber cloth electrodes for supercapacitors. *Journal of Physical Chemistry C* 2011; **115**:23584–23590.
19. Mondal SK, Barai K, Munichandraiah N. High capacitance properties of polyaniline by electrochemical deposition on a porous carbon substrate. *Electrochimica Acta* 2007; **52**:3258–3264.
20. Zhang Y, Feng H, Wu X, Wang L, Zhang A, Xia T, Dong H, Li X, Zhang L. Progress of electrochemical capacitor electrode materials: a review. *International Journal of Hydrogen Energy* 2009; **34**:4889–4899.
21. Cai JJ, Kong LB, Zhang J, Luo YCh, Kang L. A novel polyaniline/mesoporous carbon nano-composite electrode for asymmetric supercapacitor. *Chinese Chemical Letters* 2010; **21**:1509–1512.
22. Ganesh V, Pitchumani S, Lakshminarayanan V. New symmetric and asymmetric supercapacitors based on high surface area porous nickel and activated carbon. *Journal of Power Sources* 2006; **158**:1523–1532.
23. Shi Ch, Zhao Q, Li H, Liao Z-M, Yu D. Low cost and flexible mesh-based supercapacitors for promising large-area flexible/wearable energy storage. *Nano Energy* 2014; **6**:82–91.
24. Chee WK, Lim HN, Huang NM. Electrochemical properties of free-standing polypyrrole/graphene oxide/zinc oxide flexible supercapacitor. *International Journal of Energy Research* 2015; **39**:111–119.
25. Adekunle AS, Ozoemena KI, Mamba BB, Agboola BO, Oluwatobi OS. Supercapacitive properties of symmetry and the asymmetry two electrode coin type supercapacitor cells made from MWCNTS/nickel oxide nanocomposites. *International Journal of Electrochemical Science* 2011; **6**:4760–4774.
26. Zhou C, Han J, Guo R. Synthesis of polyaniline hierarchical structures in a dilute SDS/HCl solution: nanostructure covered rectangular tubes. *Macromolecules* 2009; **42**:1252–1257.
27. Stejskal J, Sapurina I, Trchova M, Konyushenko EN, Holler P. The genesis of polyaniline nanotubes. *Polymer* 2006; **47**:8253–8262.
28. Zujovic ZD, Laslau C, Bowmaker GA, Kilmartin PA, Webber AL, Brown SP. Role of aniline oligomeric nanosheets in the formation of polyaniline nanotubes. *Macromolecules* 2010; **43**:662–670.
29. Reddy KR, Sin BC, Ryu KS, Noh J, Lee Y. In situ self-organization of carbon black-polyaniline composites from nanospheres to nanorods: synthesis, morphology, structure and electrical conductivity. *Synthetic Metals* 2009; **159**:1934–1939.
30. Ghosh D, Giri S, Kalra S, Das ChK. Synthesis and characterisations of TiO_2 coated multiwalled carbon nanotubes/graphene/polyaniline nanocomposite for supercapacitor applications. *Open J. Applied Sciences* 2012; **2**:70–77.
31. Senthilkumar ST, Selvan RK, Ulaganathan M, Melo JS. Fabrication of Bi_2O_3||AC asymmetric supercapacitor with redox additive aqueous electrolyte and its improved electrochemical performances. *Electrochimica Acta* 2014; **115**:518–524.
32. Wang Y, Shi Z, Huang Y, Ma Y, Wang C, Chen M, Chen Y. Supercapacitor devices based on graphene materials. *Journal of Physical Chemistry C* 2009; **113**:13103–13107.